Modeling of viscous behavior of rocks for deep tunnels

M. Sahli
Ecole Hassania des Trvaux Publics, casablanca

F. Pellet, E. Boidy & G. Fabre
Laboratory 3S, University of Grenoble, France

ABSTRACT: Lemaitre viscoplastic law, as a suitable viscous model for deep underground openings is developed in this paper. This model is implemented in a finite difference code for use in research and engineering projects. Different laboratory testing paths for the determination of viscous media parameters, applied for a sandstone and a shale, are given. Since experimental duration is material and path dependent, we are discussing how specimen-testing time, during primary creep can be shortened with no more information loss. This theoretical model was applied to simulate a deep circular tunnel. Stress relaxation at the tunnel wall was highlighted as well as time dependent gallery closure. It is intended to achieve the code implementation, by taking into account the secondary creep behavior, to compare monitoring data of existing tunnels, as a back computational analysis for validation of such model.

1 INTRODUCTION

Delayed convergence of deep tunnels can occur for a long duration. Monitoring this behaviour in existing openings is a useful data basis for back analysis computations. To do so, material mechanical behaviour is to be defined, and viscous parameters be determined. As an example, in Malabata experimental shaft for Gibraltar strait project, at 157 and 300 m depth in shale, gallery's convergence measures showed an important section closure within time (Hammoud, 1998).

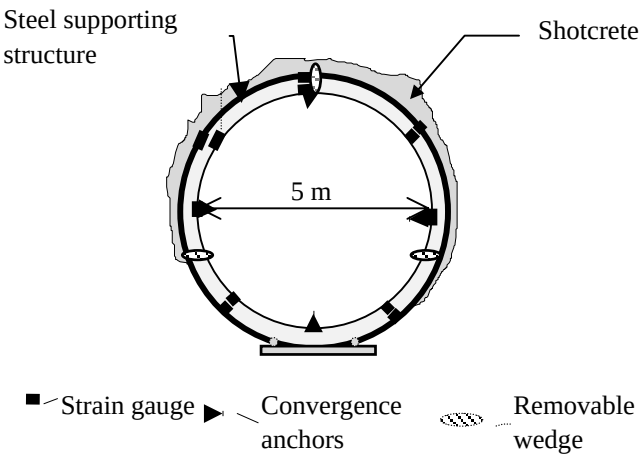

Figure 1. Malabata experimental gallery at 300 m depth (SNED)

To prevent the lining damage at gallery's wall, three removable wedges were inserted within the steel structure (Figure 1). The step 1 acceleration given in Figure 2 corresponds to the removal of the first wedge, then step 2 to the removal of second wedge and so on.

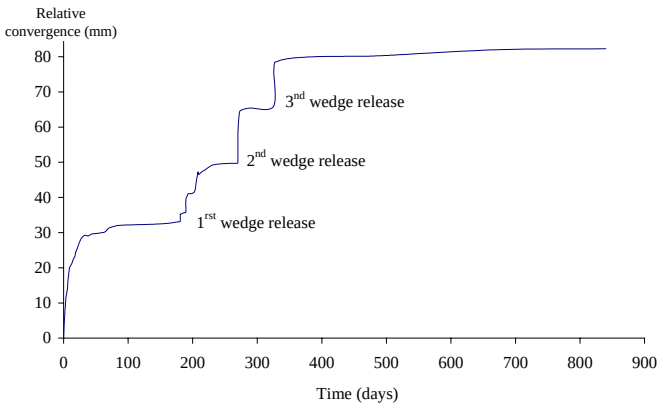

Figure 2. Relative convergence measures at –300 m in the Malabata experimental gallery for the Gibraltar strait project (SNED data)

For the strait link project, the delayed convergence knowledge is considered, in actual preliminary study, as a fundamental condition to insure the long-term stability of the tunnel.

2 VISCOPLASTIC TESTING BEHAVIOUR

Primary creep tests on many rocks have been reported to fit a power law with respect to time (Sahli, 1990). Creep of rocks can be shown experimentally by carrying up tests on different paths. In constant strain rate paths to failure, higher strain rates values end in low viscoplastic strains while for very low strain rate viscoplastic behaviour is observed. For experimental creep paths at constant stress tensor increase of strain with time is due to the viscous behaviour. In relaxation tests, at a constant total axial strain, total lateral strain and the whole viscoplastic tensor strain are free to vary with increasing time. Three stages of material response are usually observed (Figure 3): -the primary (or transient) creep occuring at high decreasing strain rate, -the secondary creep at a constant strain rate, -and the damage of material when the tertiary stage is occurring. Some authors define stress threshold values for these behaviours (Laigle & Kolmayer, 1998).

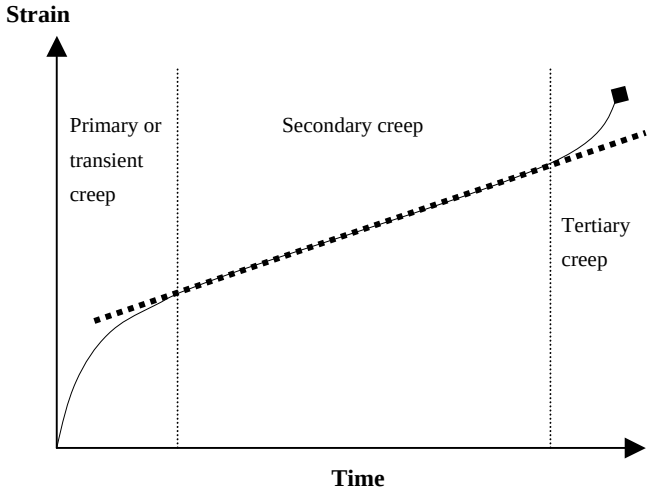

Figure 3. Creep stage behaviours (under constant loading)

3 VISCOPLASTIC LAW

Lemaitre & Chaboche (1996) previously presented a three-dimensional generalised viscoplastic flow rule for primary creep, derived from a potential.

3.1 *Tensor strain partition*

Partition of total tensor strains assumed by authors involves two terms: the instantaneous strains term and the viscoplastic strains.
Since for our purpose, loading paths are monotonic, instantaneous strains are kept together and denoted $\underline{\varepsilon}^{ep}$, while viscoplastic strains are the sum of purely plastic and anelastic strains, this latter being assumed negligible. Partition condition for small deformations within viscoplastic behaviour leads finally to:

$$\underline{\varepsilon} = \underline{\varepsilon}^{ep} + \underline{\varepsilon}^{vp} \tag{1}$$

where $\underline{\varepsilon}$ = the total strain tensor at a given time; $\underline{\varepsilon}^{ep}$ = the time independent strain part; $\underline{\varepsilon}^{vp}$ = the viscoplastic strain tensor.

Our study is restricted to the analysis of the first and second stages of the behaviour. Hence experimental loading results considered are under the material damage threshold, defined as the initiating of microstructure growth and volume changes limit discussed by Thorel & Ghoreychi (1996). The transient creep involves a hardening phenomena, corresponding to microstructure changes during specimen loading (as gliding, deviation, etc..), while ageing and recovery are assumed to be not present. In respect with these assumptions, the isotropic hardening parameter can be chosen as a viscoplastic strain scalar functional p, defined by:

$$p = \int_0^t \left(\frac{2}{3} \dot{\varepsilon}_{ij}^{vp} \cdot \dot{\varepsilon}_{ij}^{vp} \right)^{\frac{1}{2}} d\tau \tag{1}$$

3.2 *Lemaitre viscoplastic law*

Lemaitre generalised viscoplastic flow rule is deriving from a dissipation potential. Hence, the material deforming occurs with respect to the second principle of thermodynamics. For an isotropic material with an existing initial relaxed configuration, and no temperature changes, thermodynamic independent variables are reduced to the total strain tensor, while viscoplastic strain tensor is an internal variable (describing the actual deforming state). As we deal with a dissipating process, one can define a dissipating pseudo-potential, denoted $\varphi = \varphi(\underline{\sigma}, R, p)$, where R is the isotropic hardening variable. Normality rules then allow following relations:
Viscoplastic strain rate tensor:

$$\dot{\underline{\varepsilon}}^{vp} = \frac{\partial \varphi}{\partial \underline{\sigma}} \tag{2}$$

Isotropic hardening parameter rate:

$$\dot{p} = -\frac{\partial \varphi}{\partial R} \tag{3}$$

Since the material is isotropic, φ can be expressed as a function of the three stress invariants. Furthermore, because of experimental evidence, the third stress invariant effect can be neglected, and for viscoplastic incompressible behavior (assumed for hard rocks), the first stress invariant has no more influence on the dissipating potential function. φ is then function of the second deviator stress tensor invari-

ant, denoted J_2. By using normality rule, following relation is obtained:

$$\underline{\dot{\varepsilon}}^{vp} = \frac{3}{2}\dot{p}\frac{\underline{s}}{J_2} \tag{4}$$

where $\underline{s} = \underline{\sigma} - 1/3\ \sigma_{ii}.\underline{\delta}$; $\underline{\delta}$ = the identity tensor.

Lemaitre & Chaboche, assume a mathematical dissipation function for the transient creep, in case of no threshold, as follows:

$$\varphi = \frac{K}{n+1}\cdot\left\langle\frac{J_2}{K}\right\rangle^{n+1}\cdot p^m \tag{5}$$

where K = scalar constant; <x> = 0 for x<0 and <x> = x for x>0.

Hence, constitutive equation of the viscoplastic strain rate tensor is:

$$\underline{\dot{\varepsilon}}^{vp} = \frac{3}{2}\cdot K^{-n}\cdot {J_2}^{n}\cdot p^m\cdot\frac{\underline{s}}{J_2} \tag{6}$$

3.3 *Material constant determination*

Equation 6 describes the isotropic viscous material behaviour, through three material constants: K, n and m. Parameter's determination can be done after laboratory tests on material specimens, carried out on simplest, shortest paths. For triaxial tests carried out on cylindrical specimens, with the vertical axis being a principle direction for isotropic materials, lateral directions are identical. Since the viscoplastic incompressibility condition is assumed, viscoplastic lateral deformation is related to the axial one (denoted *I*) through following expression:

$${\varepsilon_{II}}^{vp} = {\varepsilon_{III}}^{vp} = -\frac{1}{2}\cdot{\varepsilon_I}^{vp} \tag{7}$$

while hardening parameter expression reduces to:

$$p = \int_0^t \left|{\dot{\varepsilon}_I}^{vp}\right| d\tau \tag{8}$$

Second invariant tensor expression is:

$$J_2 = \left[\frac{3}{2}\,\underline{s}:\underline{s}\right]^{\frac{1}{2}} = \left|\sigma_I - \sigma_{III}\right| \tag{9}$$

For monotonic uniaxial compression tests, Equation 6 reduces to:

$${\dot{\varepsilon}_I}^{vp} = \left(\frac{\sigma_I}{K}\right)^n\cdot\left({\varepsilon_I}^{vp}\right)^m\cdot \tag{10}$$

Integrating along a purely creep path ends in:

$${\varepsilon_I}^{vp} = A\cdot{\sigma_I}^{\beta}\cdot t^{\alpha} \tag{11}$$

Creep test data give the time exponent as a tendency curve slope in a log-log axes. When a set of curves are carried out for different constant stress values, one can by a similar way find the stress exponent and the coefficient A values. For rocks in study, this latter parameter is very small, we define instead the parameter *a* given by Equation 12:

$$a = \left(\frac{A}{\alpha}\right)^{\alpha} \tag{12}$$

Along with experimental relaxation path, for each curve carried out at a constant axial strain ${\varepsilon_I}^0$, we have at any time

$${\varepsilon_I}^0 = \frac{\sigma_I}{E} + {\varepsilon_I}^{vp} \tag{13}$$

and by deriving with respect to time,

$${\dot{\varepsilon}_I}^{vp} = -\frac{\dot{\sigma}_I}{E} \tag{14}$$

where E is the material monotonic loading modulus.

In case of tests with constant total strain rate, we have, instead

$${\dot{\varepsilon}_I}^0 = \frac{\dot{\sigma}_I}{E} + {\dot{\varepsilon}_I}^{vp} \tag{15}$$

For both the two latter test paths, there is no analytically simple expression, giving the time-dependent response. However, for a set of data on a given path, we point out a useful fitting method, using the logarithmic expression of Equation 10, that is:

$$\ln\left({\dot{\varepsilon}_I}^{vp}\right) = n\left[\ln(\sigma_I) - \ln K\right] + m\ln\left({\varepsilon_I}^{vp}\right) \tag{16}$$

3.4 *Path delayed equivalent time*

For primary creep, the three tensor variables $\underline{\varepsilon}^{vp}$, its time derivative and stress tensor $\underline{\sigma}$ are all related at any time through an analytical expression given by Equation 6, no matter could be the loading path. For a given state, namely $\{{\varepsilon_I}^{vp,*}, {\sigma_I}^*\}$, time to reach the given variables set is depending on the chosen path. For the uniaxial creep path, time is:

$$T_f = \frac{\left({\varepsilon_I}^{vp,*}\right)^{1-m}}{(1-m)\left(\frac{\sigma^*}{K}\right)^n} \tag{17}$$

while for a relaxation path,

$$T_r = \frac{I({\varepsilon_I}^{vp,*})}{\left(\frac{E}{K}\right)^n} \tag{18}$$

where T_f = equivalent time on creep path; T_r = equivalent time on relaxation path. Numerator for right term of Equation 18 is given below:

$$I({\varepsilon_I}^{vp,*}) = \int_0^{{\varepsilon_I}^{vp,*}} \frac{dx}{x^m\cdot\left({\varepsilon_I}^0 - x\right)^n} \tag{19}$$

Comparing the two time's values T_f and T_r gives the shortest way to carry out laboratory tests for a $\{\varepsilon_I^{vp,*},\sigma_I^*\}$ set, along with primary creep path.

4 EXPERIMENTAL RESULTS

Laboratory investigations are carried out on two rock specimens. These are an homogeneous isotropic sandstone from Villarlod site in Switzerland, and a shale from the east of France. For both materials, initial porosity is close to 19% , temperature and water content during loading were under control. However the two material compositions and derived viscoplastic behaviour are different.

4.1 *Material description*

Table 1 below summarizes physical and mechanical values for the rock materials tested.

Table 1. Identification of materials: physical parameters, maximum water content, uniaxial compression strength and loading modulus

Rock	density	porosity (%)	w_{sat} (%)	σ_c (MPa)	E (MPa)
Sandstone	2.2	17	6	11.5 - 13	2200
Shale	2.2	18 - 19	9 - 10	36.	3600 - 8000

4.2 *Villarlod sandstone results*

Uniaxial constant strain rate tests are carried out with total axial strain rates ranging from $4\ 10^{-3}$ to $3\ 10^{-6}\ s^{-1}$ (Figure 4) . Number of specimens per strain rate varies from 4 to 8. Several uniaxial creep tests were also carried out on the same rock during several days, under constant stresses, varying from 3.5 to 8.7 MPa (Sahli 1990, Pellet et al. 2000). Only primary creep was observed for all specimens tested. Fitting the experimental measures gives up the average values of parameters a, α and β as shown in Table 2.

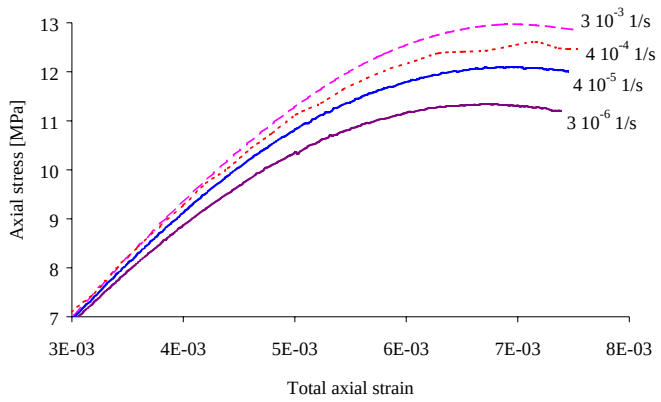

Figure 4. Stress-strain curves for different strain rates on sandstone

Table 2. Lemaitre power Law constants, given by fitting creep tests on a sandstone

	a [MPa, days]	α	β	n	m
Average value	$3.35\ 10^{-5}$	$7.36\ 10^{-2}$	1.49	21.11	-13.20
Variation coefficient	25.5%	21.4%	1.2%	21.9%	23.4%

Since both axial and lateral strains are simultaneously monitored within time, volume variation during creep was also determined. Assumption of primary creep behavior occurrence with no significant volume change, during the delayed process is confirmed for the sandstone tested (Table 3).

Table 3. Volumetric variation coefficients (instantaneous ν_{init} and viscoplastic ν_{vp}), obtained by fitting creep tests on a sandstone

	ν_{init}	ν_{vp}
Average value	0.39	0.48
Variation coefficient	21.9 %	17.6 %

Comparison between creep and relaxation paths can be made in term of quickness to attend a $\{\varepsilon_I^{vp,*},\sigma_I^*\}$ set values. Conclusion is that creep tests are about 20 to 28 % slower than relaxation tests, in term of equivalent times to reach a given state, as shown in Table 4.

Table 4. Relative equivalent time to reach a given state along with creep or relaxation path (primary creep of sandstone)

ε_I^{vp}	σ_I [MPa]	Tf/Tr
$2.5\ 10^{-4}$	3.5	1.24
$5.0\ 10^{-4}$	6.0	1.28
$6.0\ 10^{-4}$	10.0	1.20

4.3 *Shales from the east of France*

Few unpublished creep tests were carried out on this material and a set of Lemaitre parameters previously determined. Using these values for equivalent time calculations ends in equivalent time's ratio varying from 3 to 5. Hence, a relaxation-testing program was preferred since these tests are shorter. An example of the relaxation test is given in Figure 5.

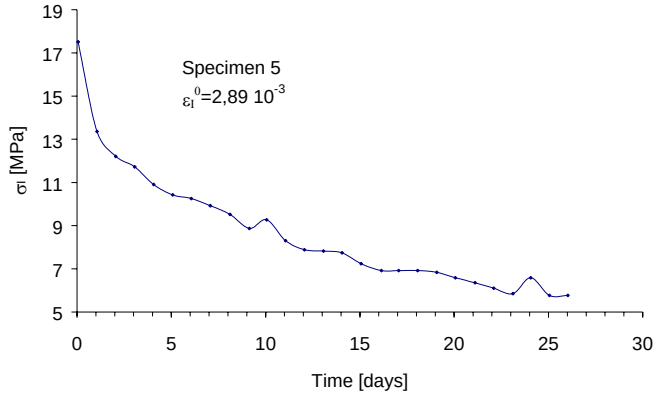

Figure 5. Relaxation curve on shale

Constant strain rate tests were also carried out under a wide range of deformation rates, from 10^{-9} to 10^{-3} s^{-1}. As a result of Equation 16, all experimental data can be gathered together in a log-log diagram. Parameters finally obtained for the material are n= 9.25; m= -1.77; *a*= 8.25 10^{-8} (MPa, days) (Boidy & Pellet 2000). As a result, final equivalent time calculations are given in the Table 5.

Table 5 : Relative equivalent times to reach a given state along with creep or relaxation path (primary creep of shale)

E [MPa]	ε_I^{vp}	σ_I [MPa]	Tf/Tr
7500	1.6 10^{-3}	10	3.84
7500	2.4 10^{-3}	17	3.22
4700	5.3 10^{-3}	15	4.96

Relaxation tests show a secondary creep appearance after approximately one week of loading. By equation 14, we conclude for the secondary creep behaviour to occur also at the same stress and strain set of values (i.e. ε_I^{vp}=1.6 10^{-3}, s_I=10 MPa). By using Table 5, one can then estimate the creep time appearance, which is close to 4 weeks.

We conclude from these testing programs that Villarlod sandstone has a fair ability to creep with respect to time. In contrast, shale exhibits a great tendency to deform. Furthermore, with one-month duration testing, the shale behaviour is yet a steady-state creep

5 NUMERICAL SIMULATION

The Lemaitre viscous law for primary creep behaviour was implemented in a 2D-FLAC numerical code, using a proper internal code language (Boidy & al. 2001). An underground-unlined circular tunnel is simulated at 300 depth, in sandstone and a shale material discussed in this paper. Initial stresses are assumed to be isotropic, and gravity effect negligible. Mesh discretisation and other assumptions, so as boundary conditions are summarised in Figure 6.

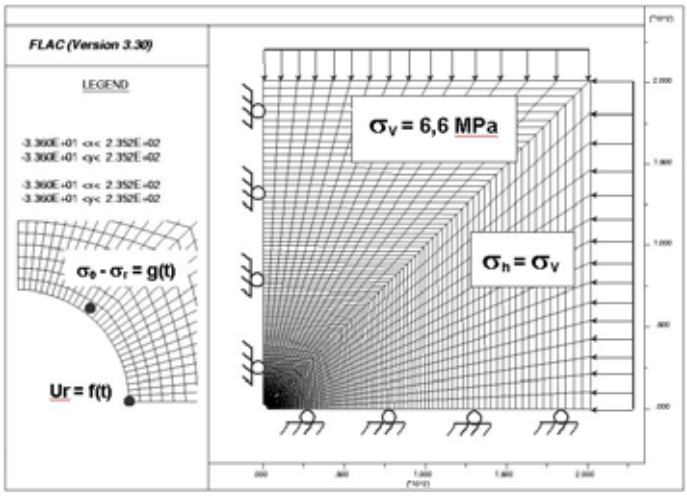

Figure 6. Tunnel mesh discretisation and boundary conditions

Stress relaxation and total strains at the simulated tunnel wall during 4 years, are given in Figure 7 for the sandstone and in Figure 8 for the shale. These curves show a more important tunnel closure with the shale surrounding material, and an amount shear stress decrease of 30 %.

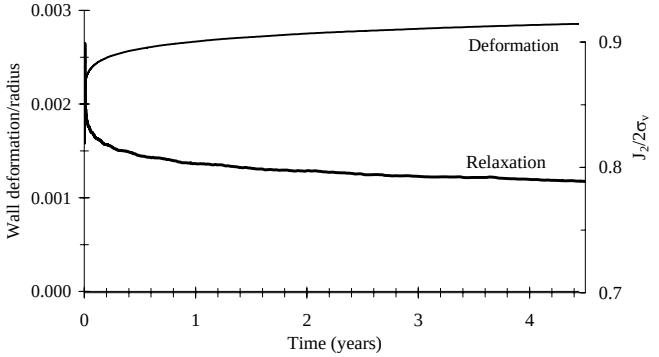

Figure 7. Time-dependent relaxation and closure of a deep tunnel facing in sandstone

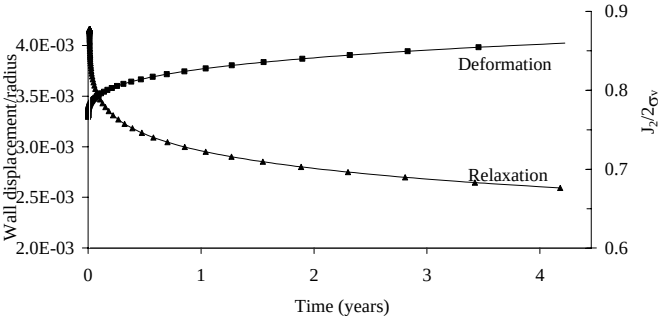

Figure 8. Time-dependent relaxation and closure of a deep tunnel facing in the shale

In Figure 9 are plotted the radial displacements at different distances from the tunnel axis excavated in shale, for periods going from 1 day to 4 years. These curves show an important change in convergence values from the wall tunnel to a distance of 20 m in the rock mass. However, delayed strains are observed in all the rock mass, with a fair decrease when distance from the tunnel axis increases.

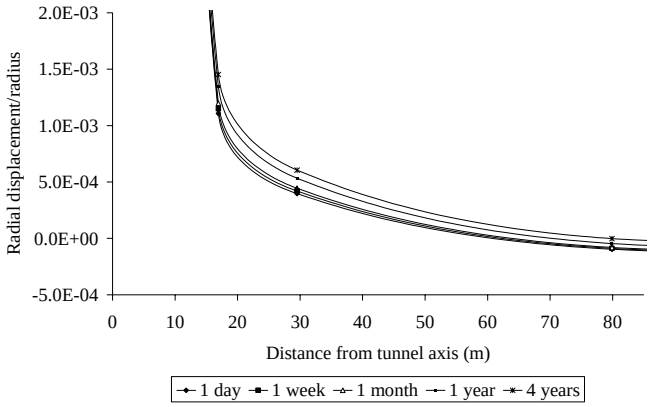

Figure 9. Dimensionless radial displacements of grid points of the simulated tunnel in the shale

In Figure 10, the relaxation of J_2 deviator for some elements of the mesh is given as a function of the distance from the tunnel axis. This figure shows an important decrease of stresses with time at the vicinity of the excavation. Stress deviator at the wall decreases to half its initial value after 4 years for an unlined tunnel. This stress-delayed change is relevant for a radius of 15 m in rock mass.

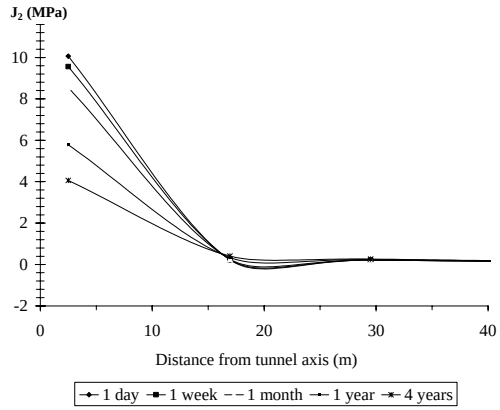

Figure 10. Relaxation of the stress deviator of the simulated tunnel in the shale

6 CONCLUSION

A viscoplastic formulation law for viscous rocks before damage is given. Different laboratory testing paths are used for the parameter determination of a fairly viscous sandstone from Villarlod in Switzerland and a mid viscous shale rock from the east of France. Best laboratory testing paths in term of gain of time are discussed. The primary creep model is implemented in a finite difference code and applied to tunnel at 300 m depth. However, a suitable numerical simulation for real projects has to take into account the secondary creep behaviour. This focus is under achievement with objective of a back computational analysis of the Malabata and East France waste disposal as two examples of deep underground projects.

REFERENCES

Boidy, E., Pellet, F.& Boulon, M. 2001. Numerical modelling of deep tunnels including time-dependent behaviour. Proc. 10th Int. Conf. IACMAG, Tucson, USA.

Boidy, E. & Pellet, F. 2000. Identification of mechanical parameters for modeling time-dependent behavior of shales. In ANDRA Workshop, *Behaviour of deep argillaceous rocks: Theory and experiment; Proc. Int. Workshop on Geomech., Paris, 11-12 October 2000*.

Hammoud, I. 1998. *Comportement des galeries dans l'argile profonde (tunnel sous le Détroit de Gibraltar)*, Thèse de Doctorat, Ecole Centrale de Paris, 204 pp, 1998

Laigle, F. & Kolmayer, P. 1998. Numerical modelisation for long term behaviour of underground structures [In French]. *Revue Française de Géotechnique* 85: 65-78.

Lemaitre, J. & Chaboche, J.L. 1996. Mécanique des matériaux solides. Paris : Dunod.

Pellet, F., Sahli, M., Boidy, E.& Boulon, M. 2000. Modelling of time-dependent behaviour of sandstones for deep underground openings. Proc. Int. Conf. on Engng. and Tech. Science (ICETS 2000), Beijing, China.

Sahli, M. 1990. Quasi-static and deferred tests on sandstone [In French]. Annales de l'ITBTP., 482: 3-9

Thorel, L. & Ghoreychi, M. 1996. Plasticity and damage of rock salt [In French]. Revue Française de Géotechnique. 77: 3-17.